Acta Crystallographica Section D
Biological Crystallography
ISSN 0907-4449

Structural analysis of the L-alanoyl-D-glutamate endopeptidase domain of *Listeria* bacteriophage endolysin Ply500 reveals a new member of the LAS peptidase family

Ingo P. Korndörfer,[a]*‡ Alexander Kanitz,[a] Josef Danzer,[a] Markus Zimmer,[b] Martin J. Loessner[b] and Arne Skerra[a]*

[a]Lehrstuhl für Biologische Chemie, Technische Universität München, An der Saatzucht 5, D-85350 Freising, Germany, and [b]Institute of Food Science and Nutrition, ETH Zurich, Schmelzbergstrasse 7, CH-8092 Zurich, Switzerland

‡ Present address: Crelux GmbH, Am Klopferspitz 19a, 82152 Martinsried, Germany.

Correspondence e-mail: korndoerfer@crelux.com, skerra@wzw.tum.de

Received 9 February 2008
Accepted 23 March 2008

PDB Reference:
enzymatically active domain of Ply500, 2vo9, r2vo9sf.

Similar to many other bacterial cell-wall-hydrolyzing enzymes, the *Listeria* bacteriophage A500 endopeptidase Ply500 has a modular architecture consisting of an enzymatically active domain (EAD) linked to a cell-wall-binding domain (CBD) in a single polypeptide chain. The crystal structure of the EAD of Ply500 has been solved at 1.8 Å resolution. The shape of the enzyme resembles a sofa chair: one α-helix and three antiparallel β-strands form the seat, which is supported by two more α-helices, while another α-helix together with the following loop give rise to the backrest. A sulfate anion bound to the active site, which harbours a catalytic Zn^{2+} ion, indicates mechanistic details of the peptidase reaction, which involves a tetrahedral transition state. Despite very low sequence similarity, a clear structural relationship was detected to the peptidases VanX, DDC, MSH and MepA, which belong to the so-called 'LAS' family. Their gross functional similarity is supported by a common bound Zn^{2+} ion and a highly conserved set of coordinating residues (His80, Asp87 and His133) as well as other side chains (Arg50, Gln55, Ser78 and Asp130) in the active site. Considering the high sequence similarity to the EAD of the *Listeria* phage endopeptidase Ply118, both enzymes can thus be assigned to the LAS family. The same is the case for the L,D-endopeptidase CwlK from *Bacillus subtilis*, which shows both functional and amino-acid sequence similarity. The fact that the CBD of Ply500 is closely homologous to the CBD of the *Listeria* phage *N*-acetylmuramoyl-L-alanine amidase PlyPSA, which exhibits a totally different EAD, illustrates the modular composition and functional variability of this class of enzymes and opens interesting possibilities for protein engineering.

1. Introduction

Ply500 is a 33.4 kDa L-alanoyl-D-glutamate peptidase of bacteriophage A500, a temperate phage that infects *Listeria monocytogenes* serovar 4 strains (Loessner *et al.*, 1995). Like most other known endolysins, Ply500 has a modular architecture consisting of a C-terminal cell-wall-binding domain (CBD) and an N-terminal enzymatically active domain (EAD; Loessner *et al.*, 1995, 2002; Loessner, 2005; Korndörfer *et al.*, 2006). The CBD serves to specifically recognize and bind to the bacterial cell surface, which defines target specificity largely independently of the catalytic activity contributed by the EAD (Loessner *et al.*, 2002).

The CBD of Ply500 (residues 155–289 of the full-length enzyme; dubbed CBD500) exhibits about 70% amino-acid sequence identity to the corresponding domain of the *N*-acetylmuramoyl-L-alanine amidase PlyPSA from bacteriophage PSA, while the EADs of the two enzymes are unrelated. The crystal structure of PlyPSA has recently been elucidated and revealed a novel fold of its CBD, comprising two copies of a β-barrel-like motif that are held together *via* swapped β-strands (Korndörfer *et al.*, 2006). Based on the close sequence similarity, CBD500 is assumed to have a similar three-dimensional structure.

The L-alanoyl-D-glutamate endopeptidase activity of Ply500 has so far only been found among phages of *Listeria*. Interestingly, EAD500 (residues 1–154) displays approximately 30% amino-acid sequence identity to the corresponding functional domain of Ply118, a related peptidase from *Listeria* bacteriophage A118 (Loessner *et al.*, 1995), while the CBD domains of these two enzyme are unrelated. In addition, the L,D-endopeptidase CwlK (YcdD), which also shows clear sequence homology to EAD500, was recently described to be chromosomally encoded in *Bacillus subtilis* (Fukushima *et al.*, 2007).

Bacteriophage peptidoglycan-hydrolyzing enzymes have found several applications in biotechnology and medicine, *e.g.* for surface-decontamination purposes, for biopreservation of food and feed and as potential topical antimicrobials (for reviews, see Loessner, 2005; Hermoso *et al.*, 2007). Unfortunately, attempts to obtain crystals of the recombinant full-length Ply500 enzyme have failed, probably owing to the inherent flexibility of its two-domain architecture (Korndörfer *et al.*, 2006). However, we report here the separate cloning and purification of the enzymatically active domain (EAD500), allowing elucidation of its crystal structure at 1.8 Å resolution.

2. Experimental

2.1. Cloning, production and purification of Ply500

The coding sequence for the Ply500 endolysin was amplified from purified phage A500 DNA using the oligodeoxynucleotide primers PLY500-Bam, 5′-TCTA**GGATCC** ATG GCA TTA ACA GAG GCA TGG CT-3′, and PLY500-Sal, 5′-AAGT**GTCGAC** TTA TTT TAA GAA GTA TTC TGC TGT GT-3′, respectively (restriction sites are shown in bold; Loessner, Rees *et al.*, 1996; Loessner, Schneider *et al.*, 1996). The reaction product was digested with *Bam*HI and *Sal*I and ligated with the appropriately cut *Escherichia coli* expression vector pASK-IBA5 (IBA, Göttingen, Germany). The resulting plasmid pSPL500 encodes the full-length 289-amino-acid Ply500 as a fusion protein with an N-terminal *Strep*-tag II affinity peptide (Schmidt & Skerra, 2007). This construct was used for the generation of truncated Ply500 fragments by introducing premature ochre stop codons *via* PCR, using a common 5′-primer (ead500-f, 5′-CCA CTC CCT ATC AGT GAT AGA GAA AAG TG-3′) together with each of three 3′-antisense primers (ead500.1–141-r, 5′-GAC**CTCGAG** TTA ACT TAC AGC ATC ACA TAG TTC AAA ATG C-3′; ead500.1–151-r, 5′-GAC**CTCGAG** TTA GTT TTG TGT TGC AGC AGG GAT TTT CTC-3′; ead500.1–163-r, 5′-GAC**CTCGAG** TTA GAC TTT ACC CTC GTA ACG ATT TGA A-3′). The three corresponding N-terminal Ply500 gene fragments, EAD500(1–141), EAD500(1–151) and EAD500(1–163), were subcloned on pASK-IBA5 utilizing the *Xba*I (vector encoded) and *Xho*I restriction sites (bold). Proper composition of the resulting expression plasmids was confirmed by analytical restriction digest and DNA sequencing.

Cultures of *E. coli* K-12 strain JM83 harbouring these plasmids were grown in 6 l LB medium (Sambrook & Russell, 2001) supplemented with 100 mg l^{-1} ampicillin at a temperature of 295 K. Gene expression was induced at a cell density (OD_{550}) of 0.8 by adding 0.2 mg l^{-1} anhydrotetracycline (Skerra, 1994). After further incubation with shaking for 2.5 h, the bacterial cells were harvested by centrifugation, resuspended in 150 m*M* NaCl, 1 m*M* EDTA, 100 m*M* Tris–HCl pH 8.0 and mechanically lysed in a French pressure cell (Aminco, Rochester, New York, USA). 1.5 n*M* avidin (Sigma–Aldrich, Deisenhofen, Germany) was added to mask biotinylated host-cell proteins and the cleared whole cell extract was applied onto a chromatography column with immobilized engineered streptavidin (Schmidt & Skerra, 2007) using the same buffer. The NaCl concentration was then gradually increased to 500 m*M* in order to elute contaminating proteins associated with the bound Ply500 fragments. Finally, the recombinant protein was competitively eluted using 2.5 m*M* D-desthiobiotin (IBA, Goettingen, Germany) in the same buffer. Eluted fractions were concentrated (Amicon Centriprep 10, Millipore, Schwalbach, Germany) and applied onto a Superdex-75 gel-filtration column (Amersham Pharmacia, Uppsala, Sweden). The EAD of Ply500 eluted as a homogenous peak corresponding to the expected size of the monomeric protein fragment in all three cases. The homogeneity of the protein fractions was checked by SDS–PAGE. Yields of purified protein were 0.6, 1.0 and 1.1 mg per litre of of *E. coli* culture at OD_{550} = 1.7 for EAD500(1–141), EAD500(1–151) and EAD500(1–163), respectively. All three recombinant fragments exhibited enzymatic activity in photometric lysis assays based on turbidity measurements with intact cells of *L. monocytogenes* strain WSLC 1042 as substrate (Loessner, Rees *et al.*, 1996).

The SeMet derivative of the EAD500(1–163) fragment was prepared by repression of bacterial methionine biosynthesis and complementation of the growth medium (Van Duyne *et al.*, 1993). For this purpose, *E. coli* K-12 strain W3110 harbouring the corresponding expression plasmid was grown in glucose M9 minimal medium (Sambrook & Russell, 2001) and L-Lys, L-Thr, L-Phe (50 mg l^{-1} each), L-Leu, L-Ile, L-Val (25 mg l^{-1} each) as well as L-SeMet (25 mg l^{-1}) were added at OD_{550} = 0.8. After 15 min incubation, plasmid-mediated gene expression was induced by adding 0.2 mg l^{-1} anhydrotetracycline. The cells were harvested after further shaking at 295 K for 6 h and the Ply500 fragment was purified as above with the addition of 1 m*M* dithiothreitol to all buffers. Incorporation of SeMet into the recombinant EAD at four sites was confirmed by MALDI–TOF mass spectrometry using a

Table 1
X-ray data-collection statistics.

Values in parentheses are for the highest resolution shell.

Data set	SeMet (peak, 0.9798 Å)	Native (1.5418 Å)
Space group	$C222_1$	$C222_1$
Unit-cell parameters (Å)	a = 59.9, b = 95.7, c = 183.7	a = 59.8, b = 95.2, c = 182.6
V_M (Å^3 Da^{-1})	2.4	2.4
No. of reflections	19662 (2758)	46858 (7003)
Resolution (Å)	40.00–2.36 (2.48 2.36)	25.00–1.80 (1.90–1.80)
Completeness of data (%)	99.4 (96.0)	96.7 (99.9)
$I/\sigma(I)$	11.9 (5.5)	23.7 (9.6)
Anomalous completeness (%)	99.1 (93.9)	—
Redundancy	10.3 (9.1)	3.7 (3.3)
R_{meas}	0.117 (0.386)	0.060 (0.242)

Table 2
Refinement statistics for the native data set.

Values in parentheses are for the highest resolution shell.

Resolution (Å)	20.00–1.80 (1.85–1.80)
Reflections used	44421 (3340)
Completeness (%)	96.3 (99.8)
R/R_{free}	0.196/0.242 (0.246/0.312)
Protein residues visible	447 residues [3 × 149 per ASU]
No. of solvent molecules	370 water molecules, 3 Zn^{2+} ions, 6 sulfate ions
Mean temperature factors (Å^2)	
Protein	25.5
Water	28.8
R.m.s.d. from ideality of bond lengths (Å)	0.015
R.m.s.d. from ideality of bond angles (°)	1.436

Q-TOF Ultima API instrument (Micromass UK Ltd, Manchester, England).

2.2. Crystallization, data collection and structure determination

Large crystals of both the native recombinant Ply500 fragment EAD500(1–163) (also carrying an N-terminal *Strep*-tag II and a spacer, with a total of 13 residues) and its SeMet derivative were grown within two weeks *via* the hanging-drop vapour-diffusion technique (McPherson, 1985) using 1.7 *M* ammonium sulfate, 2.4%(*v*/*v*) PEG 400, 0.1 *M* HEPES–NaOH pH 7.5 as precipitant. 1 µl protein solution (10 mg ml^{-1} in 500 m*M* NaCl, 10 m*M* Tris–HCl pH 8.0) was mixed with 1 µl precipitant solution on a siliconized glass cover slip, followed by equilibration against 0.5 ml precipitant solution. Protein crystals were cryoprotected by adding 0.5 µl 50%(*v*/*v*) PEG 400 to the crystallization drop, were harvested using nylon loops (Hampton Research, Aliso Viejo, California, USA) and frozen in a 100 K nitrogen stream (Oxford Cryosystems, Oxford, England).

A single-wavelength anomalous data set was collected from one crystal of the SeMet derivative at BM14 (ESRF, Grenoble, France) to a resolution of 2.36 Å (Table 1). Reflection intensities were processed with *MOSFLM* and *SCALA* (Collaborative Computational Project, Number 4, 1994). The space group was determined as $C222_1$, with three molecules in the asymmetric unit. A data set from the native protein was collected in-house on a MAR Research (Hamburg, Germany) 345 mm imaging-plate detector with Cu $K\alpha$ radiation from an RU-300 rotating-anode generator (Rigaku, Tokyo, Japan) focused through Confocal Max-Flux Optics (Osmic, Troy, Michigan, USA), yielding a final resolution of 1.80 Å (Table 1).

Selenium sites were identified with *HKL2MAP* (Pape & Schneider, 2004) using the anomalous data set. Phase calculation resulted in electron density with features revealing various α-helical elements arising from three polypeptide chains in the asymmetric unit. Selenium sites were refined with *SHARP* (de La Fortelle *et al.*, 1997*a*,*b*; phasing power = 3.06, R_{Cullis} = 0.438). After solvent flattening with *SOLOMON* (Abrahams *et al.*, 1996), 419 residues (of 447 visible residues in the final structure) were modelled automatically using *ARP*/*wARP* (Perrakis *et al.*, 1999). Alternating rounds of manual rebuilding with *QUANTA* (Oldfield, 2001) and crystallographic refinement (applying loose noncrystallographic symmetry restraints between subunits *A*, *B* and *C* in *REFMAC*5; Collaborative Computational Project, Number 4, 1994) against the native data set led to the final model with an *R* factor of 0.196 (Table 2).

During manual model building a pronounced $F_o - F_c$ difference electron density was detected for a bound metal ion situated in the active site, which was later interpreted as a Zn^{2+} ion. Further pieces of difference electron density in the direct neighbourhood of the three Zn^{2+} ions were modelled as sulfate anions, in conjunction with their high concentration in the crystallization drop. Three additional sulfate anions mediate crystallographic contacts between the monomers within the asymmetric unit or their crystallographic neighbours. Water molecules were added where stereochemically plausible and where the $2F_o - F_c$ and $F_o - F_c$ difference Fourier maps revealed densities of more than 1.0σ and 3.5σ, respectively. All backbone dihedral angles fell into allowed regions of the Ramachandran plot (Ramachandran *et al.*, 1963).

Secondary-structure assignments were made with *DSSP* (Kabsch & Sander, 1983). Electrostatic surfaces were calculated with *APBS* (Baker *et al.*, 2001). Molecular models, surfaces and electron densities were depicted using *PyMOL* (DeLano, 2002) and *APBS TOOLS* (M. G. Lerner, University of Michigan).

3. Results and discussion

3.1. Protein crystallization, structure determination and quality of the final model

After extensive attempts to crystallize the full-length Ply500 protein had been unsuccessful, we focused on the enzymatically active domain (EAD500) for structure determination. Based on a sequence alignment between Ply500 and the related PlyPSA endolysin of known crystal structure (Korndörfer *et al.*, 2006; Zimmer *et al.*, 2003; Fig. 1), in which the CBD consists of residues 183–314, the corresponding CBD of Ply500 was predicted to comprise residues 155–289 with a

sequence identity of 73%. The two EADs, in contrast, do not show any significant sequence similarity.

In the crystal structure of PlyPSA, the EAD and CBD are connected *via* a short linker peptide of six residues (177–182). Since the exact length of the linker peptide in Ply500 was not apparent from the sequence comparison, we designed three truncated versions of Ply500 for expression in *E. coli*: EAD500(1–141), EAD500(1–151) and EAD500(1–163) (see Fig. 1). The three constructs were expressed as fusion proteins with an N-terminal *Strep*-tag II (Schmidt & Skerra, 2007). Recombinant proteins were purified from the bacterial whole cell extract *via* streptavidin-affinity chromatography and gel filtration, with a final yield of approximately 1 mg protein per litre of bacterial culture. The purified Ply500 fragments exhibited lytic activities in qualitative assays (not shown), although these were significantly lower compared with the full-length Ply500 enzyme, which corresponds to the fact that the CBD is required for full activity of the endolysin on its natural murein substrate (Loessner, 2005; Korndörfer *et al.*, 2006).

After sparse-matrix screening for crystallization conditions, only the longest construct resulted in crystals that were sufficiently large (400 × 100 × 100 µm) for X-ray diffraction. The phase problem was solved by SAD using similar crystals of the selenomethionine (SeMet) derivative. The initial model was refined against the native data set collected from the unlabelled protein to a resolution of 1.80 Å, resulting in an *R* factor of 0.196 and good overall stereochemistry for three polypeptide chains (dubbed *A*, *B* and *C*) in the asymmetric unit (Table 2).

The 12 residues at the N-terminus of the recombinant protein comprising the *Strep*-tag II were disordered and were not included in the structural model. Likewise, the 19 residues at the C-terminus of this enzyme fragment were also not visible in electron density. Interestingly, crystallization trials with the more truncated versions yielded significantly smaller crystals [EAD500(1–151)] or needles [EAD500(1–141)] with inferior X-ray diffraction properties.

3.2. Overall structure of the Ply500 EAD

The EAD of Ply500 assumes an overall shape similar to that of a sofa chair (Fig. 2). Helix $\alpha1$ and the three antiparallel β-strands $\beta1$, $\beta2$ and $\beta3$ form the seat, which rests on helices

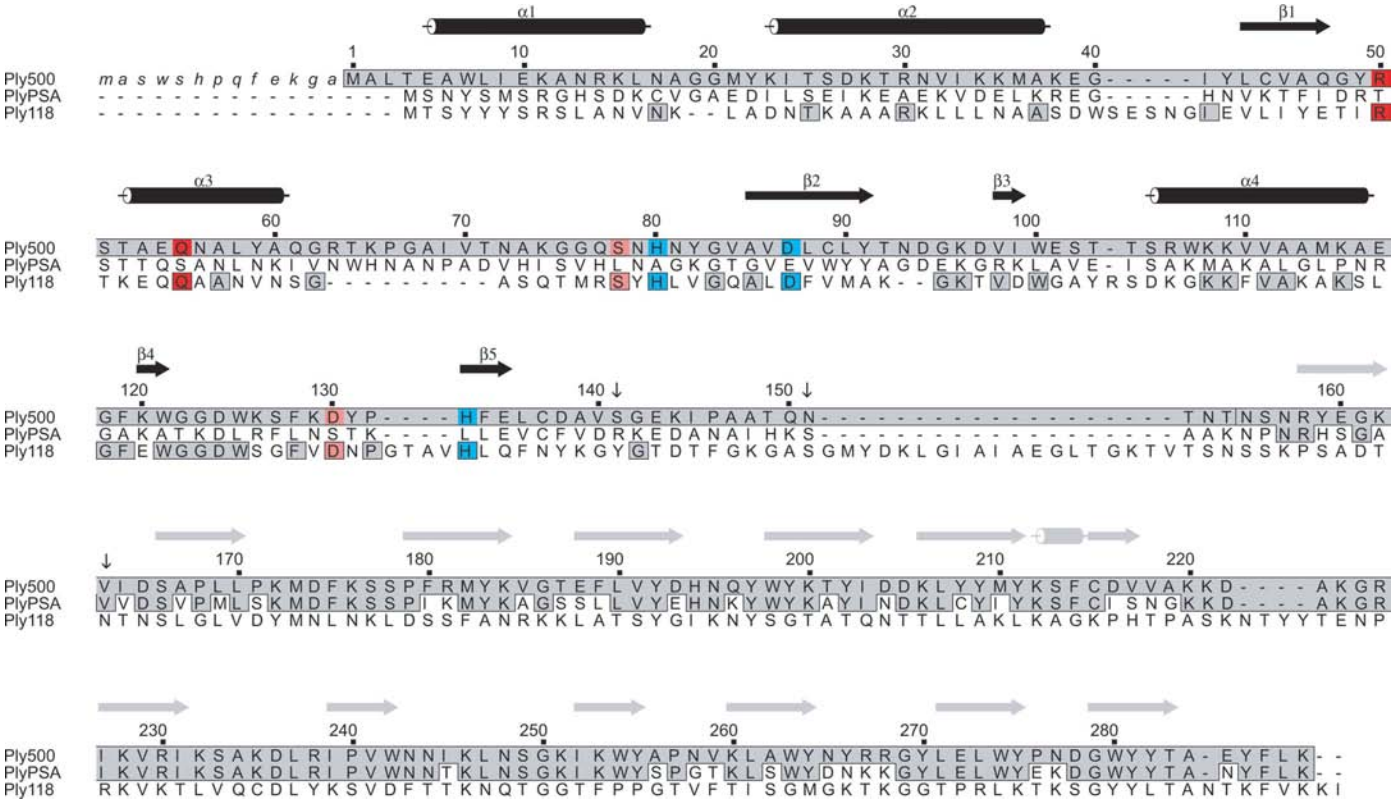

Figure 1
Alignment of the amino-acid sequence of Ply500 with the sequences of PlyPSA (PDB code 1xov) and Ply118 (Swiss-Prot accession No. Q37976). The secondary-structure assignment for the EAD500 crystal structure is indicated in black above the sequence, while secondary-structure assignments in grey are taken from the CBD in the homologous PlyPSA crystal structure. The tentative border between the EAD and CBD of Ply500 is indicated by a vertical line between residues 154 and 155. Residue numbering generally corresponds to that of the native Ply500 (without the *Strep*-tag II, which is depicted in lower-case letters at the N-terminus). The C-termini of the three constructs investigated in this work are labelled with small arrows. Mutually identical residues in the PlyPSA CBD or Ply118 EAD and corresponding regions of Ply500 are boxed in grey. Amino-acid residues involved in Zn^{2+} binding by EAD500 are highlighted in blue, together with the putative homologous residues in EAD118. Other residues relevant for catalysis are highlighted in red (those stabilizing the transition-state oxyanion) and pink (other residues).

α2 and α4. Helix α3 and the following loop (residues 62–79) give rise to the 'backrest'. A 'left armrest' of the sofa is provided by another loop (residues 125–131). Two important crystal contacts were identified. Firstly, chains *B* and *C* form a loosely packed dimer with local *C*2 symmetry *via* interaction between their α4 helices (approximately 50 Å^2 of protein surface buried). The same dimer is also formed between chain *A* and its crystallographic symmetry mate from the neighbouring asymmetric unit. Secondly, a greater contact is formed between chains *A* and *B* within the asymmetric unit (Fig. 3).

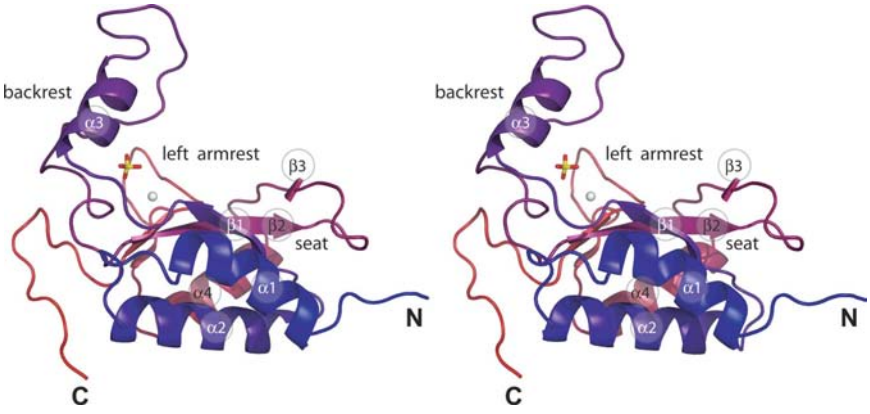

Figure 2
Overall structure of EAD500 in a stereo representation. The catalytically active Zn^{2+} ion is shown as white sphere and the neighbouring sulfate anion in the active site is depicted as a stick model. Predominant structural features are labelled (see text).

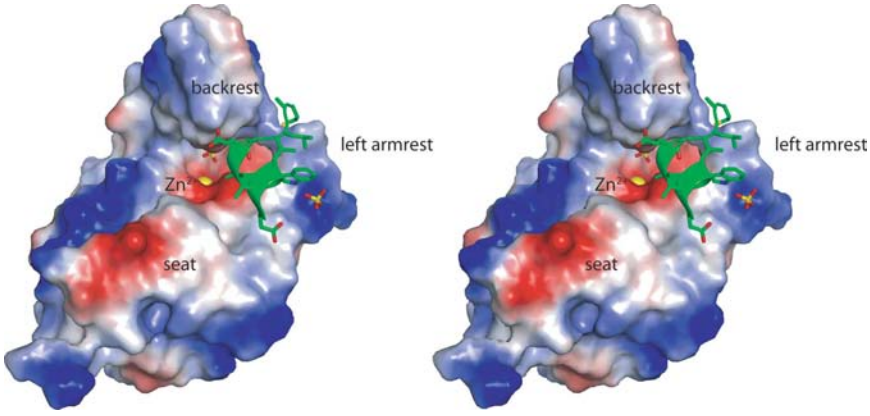

Figure 3
Crystallographic interaction between neighbouring subunits *A* (electrostatic surface representation) and *B* (green cartoon). Each polypeptide chain in the crystal structure forms contacts of this kind with its neighbour related either by crystallographic (in the case of chain *C*) or noncrystallographic symmetry (in the case of chains *A* and *B*). Thus, the sofa-like polypeptide accommodates the N-terminal peptide segment of is neighbour (residues Ala0–Glu10) between the 'backrest' and the 'left armrest'. The catalytically active Zn^{2+} ion is shown as a yellow sphere. The protein surface is coloured according to the electrostatic potential from $+50kT\ e^{-1}$ (blue) to $-50kT\ e^{-1}$ (red).

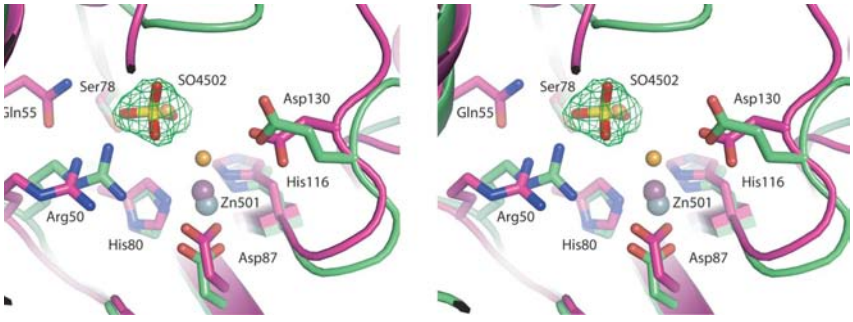

Figure 4
Superposition of the active sites between EAD500 (magenta; chain *A*) and VanX (green; PDB code 1r44). Residues of EAD500 are labelled. Zn^{2+} ions are shown as magenta and green spheres, respectively. The two small orange spheres correspond to water molecules from the VanX structure. OMIT $F_o - F_c$ electron density for the EAD500 sulfate ion, contoured at 1σ, is shown in green.

Here, chain *A* wedges its N-terminal loop (Ala0–Glu10) into the cleft between a peptide segment from the backrest (residues 67–70) and the left armrest of chain *B*. Approximately 560 Å^2 are buried in this interface and repetition of these protein subunits results in the formation of a noncrystallographic 2_1 screw axis through the crystal. Similar interactions between chain *C* and its symmetry mates form the crystallographic screw axis of space group $C222_1$. This intermolecular interaction is mostly polar in nature and involves either direct or solvent-mediated hydrogen bonds. Three sulfate anions are located within clusters of surface lysine residues (*e.g.* Lys*A*11, Lys*A*96 and Lys*B*129) at the monomer interface and thus mediate this crystallographic contact.

3.3. Structural similarities to other peptidases

A search with *DALI* (Kabsch & Sander, 1983) identified a Zn^{2+}-dependent D-alanoyl-D-alanine dipeptidase mediating vancomycin resistance (VanX) fragment from *Enterococcus faecium* (PDB code 1r44; Bussiere *et al.*, 1998; *Z* score 9.1), a D-Ala-D-Ala carboxypeptidase from *Streptomyces albus* (DDC; PDB code 1lbu; Charlier *et al.*, 2006; *Z* score 7.5), murine sonic hedgehog (MSH; PDB code 1vhh; Hall *et al.*, 1995; *Z* score 6.9) and MepA from *E. coli* (PDB code 1tzp; Marcyjaniak *et al.*, 2004; *Z* score 5.9) as the closest structural relatives. However, the amino-acid sequence identities between EAD500 and all of these enzymes are rather low according to *DALI* (DDC, 23%; VanX, 18%; MSH, 15%; MepA, 12%).

VanX, DDC, MSH and MepA share structural features, which led to their classification as 'LAS'-type enzymes, a family named according to the common arrangement of active-site residues in lysostaphin-type enzymes, D-Ala-D-Ala metalloendo-

peptidases and in the N-domain of sonic hedgehog (Bochtler *et al.*, 2004). Most of these features are also present in EAD500. LAS enzymes possess a catalytically active Zn^{2+} ion, which is tetrahedrally coordinated by two histidine side chains, an aspartate and a water molecule (*e.g.* His116, Asp123 and His184 in VanX or His154, Asp161 and His197 in DDC). The coordinating residues and their order in the amino-acid sequence are conserved in EAD500 and also in the related domain of the Ply118 endolysin (Figs. 1 and 4). The crystal structure of EAD500 shows the presence of a Zn^{2+} ion in a homologous position compared with the other LAS enzymes (distances in chain *A*: His80 NE2—Zn^{2+}, 2.0 Å; Asp87 OD2—Zn^{2+}, 2.0 Å; His133 ND1—Zn^{2+}, 2.1 Å).

According to the proposed reaction mechanism for VanX (Matthews *et al.*, 2006) as well as for MepA (Marcyjaniak *et al.*, 2004), the coordinating water molecule is activated by the Zn^{2+} ion together with another residue that acts as a general base (Glu181 in VanX) to promote nucleophilic attack of the substrate peptide carbonyl group. The resulting tetrahedral intermediate is again stabilized by the Zn^{2+} ion. Glu181 is replaced by the similarly acidic residue Asp130 in EAD500. The sulfate anion in the direct neighbourhood (distance: SO4 O1—Zn^{2+}, 3.7 Å) seems to mimic the tetrahedral transition state of the peptidase reaction. In this scenario, Arg50 (corresponding to Arg71 in VanX, Arg138 in DDC and His135 in MSH; distance: Arg50 NH1—SO4 O4, 3.3 Å) as well as Gln55 (distance: Gln55 NE2—SO4 O4, 3.2 Å) of Ply500 could further stabilize the oxyanion in EAD500 and might also contribute to the differing substrate specificity compared with VanX.

As in the other LAS enzymes, the active-site residues are located on a β-sheet, with the exception of His80, which is usually part of the loop connecting strands $\beta1$ and $\beta2$. Thus, in Ply500 the active site lies in the crease formed by residues from the seat (Asp87 and His133) and from the backrest (His80) of the sofa chair. Closely upstream of the last histidine residue, most LAS enzymes exhibit a third histidine residue (*e.g.* His195 in DDC, His181 in MSH or His209 in MepA; Bochtler *et al.*, 2004), which has been proposed to interact with the transition state. However, this third histidine is absent in both EAD500 and in VanX. Whereas the active sites of EAD500 and VanX are highly homologous, the loops that line the active-site entrances in the two enzymes assume vastly different conformations and seem to be responsible for their differing specificities. The active site of EAD500 is widely accessible to the peptidoglycan substrate from both the seat and through the gap between the backrest and the left armrest of the sofa-like structure (Fig. 3), especially as the latter can be expected to display some flexibility in solution. In VanX, only a narrow channel from the back side allows access of its known dipeptide substrate to the active site.

Recently, the CwlK (YcdD) gene product of *B. subtilis* was reported to be an L,D-endopeptidase with peptidoglycan-hydrolyzing activity (Fukushima *et al.*, 2007). In contrast to the Ply500 from *Listeria* phage, this enzyme of 167 residues is encoded on a bacterial chromosome and is secreted during the vegetative growth phase to function in restructuring the cell-wall peptidoglycan. Similarly, however, it has specificity for the L-alanoyl-D-glutamic acid linkage. The mature part of CwlK (27–167) is highly homologous to EAD500, with 49% amino-acid identity. In addition, all the critical active-site residues described here are conserved. Thus, the *B. subtilus* enzyme CwlK obviously represents another new member of the LAS family.

3.4. Implications for the enzymatic mechanism

Notably, the observed crystal-packing interaction between the N-terminal peptide segment of Ply500 and the backrest of its neighbouring EAD does not occur close enough to the active site to allow cleavage of a peptide bond. All residues of this peptide segment are more than 12 Å away from the catalytically active Zn^{2+} ion. This kind of interaction cannot therefore serve to actually recognize the peptide substrate for enzymatic hydrolysis. Nevertheless, this mode of binding might be employed to bind to the bacterial cell-wall target *via* more remote peptide and/or sugar stretches. Alternatively, the backrest and left armrest may display sufficient flexibility in solution to provide better access to the active site.

Calculation of the electrostatic surface potential reveals a predominantly positively charged surface with a negatively charged path across the seat of the sofa, which passes through an opening in the backrest where the catalytically active Zn^{2+} ion is located (Fig. 3). At present, it is not clear how this feature contributes to the substrate specificity and catalytic activity of Ply500.

EAD500 shows about 30% amino-acid identity to the corresponding domain of Ply118. All the key residues of Ply500 that are involved in binding of the catalytically active Zn^{2+} ion and identify its EAD as an LAS protein are conserved in Ply118 (Fig. 1). While no structural information is available to date for Ply118, its EAD can be expected to assume a very similar fold to EAD500 and thus also seems to belong to the LAS family. In contrast, the EAD of PlyPSA endolysin, the CBD of which is homologous to that of Ply500 (Fig. 1), shows an entirely different fold with a twisted six-stranded β-sheet flanked by six α-helices as the core structure. Furthermore, being an *N*-acetylmuramoyl-L-alanine amidase, this enzyme exhibits a different catalytic mechanism, although again with a bound Zn^{2+} ion in its active site.

In conclusion, Ply500 displays a modular architecture comprising largely independent CBD and EAD moieties, which are connected *via* a short linker peptide (Korndörfer *et al.*, 2006). The amino-acid sequence of CBD500 is almost identical to that of the corresponding CBD of PlyPSA and it most probably assumes the same three-dimensional fold. However, in contrast to PlyPSA, EAD500 is an endopeptidase with strong similarity to the well characterized LAS-type enzymes. This structural relatedness clearly illustrates that the enzymatically active domains and the cell-wall-binding domains of the *Listeria* phage endolysins have evolved independently and suggests that both domains may be exchanged without severe functional limitations. This not only explains the great variety of these enzymes found in bacteriophages,

but also opens prospects for achieving novel useful functions *via* protein engineering.

We thank I. Theobald, TU München for providing the streptavidin-affinity column, H. Stalz, TU München for mass spectrometry of SeMet variants and the European Molecular Biology Laboratory Grenoble Outstation, in particular M. Walsh, for supporting the X-ray measurements at the European Synchrotron Radiation Facility under the 'Improving Human Potential Programme' of the European Union. We are grateful to S. Scherer, TU München for support during the initial phase of this project.

References

Abrahams, J. P., Buchanan, S. K., Van Raaij, M. J., Fearnley, I. M., Leslie, A. G. & Walker, J. E. (1996). *Proc. Natl Acad. Sci. USA*, **93**, 9420–9424.

Baker, N. A., Sept, D., Joseph, S., Holst, M. J. & McCammon, J. A. (2001). *Proc. Natl Acad. Sci. USA*, **98**, 10037–10041.

Bochtler, M., Odintsov, S. G., Marcyjaniak, M. & Sabala, I. (2004). *Protein Sci.* **13**, 854–861.

Bussiere, D. E., Pratt, S. D., Katz, L., Severin, J. M., Holzman, T. & Park, C. H. (1998). *Mol. Cell*, **2**, 75–84.

Charlier, P., Wery, J.-P., Dideberg, O. & Frère, J.-M. (2006). *Streptomyces albus G* D-*Ala*-D-*Ala Carboxypeptidase.* In *Handbook of Metalloproteins*, Vol. 3, edited by A. Messerschmidt, T. Poulos, K. Wieghardt, M. Cygler & W. Bode. New York: John Wiley & Sons.

Collaborative Computational Project, Number 4 (1994). *Acta Cryst.* D**50**, 760–763.

DeLano, W. L. (2002). *The PyMOL Molecular Graphics System.* http://www.pymol.org.

Fukushima, T., Yao, Y., Kitajima, T., Yamamoto, H. & Sekiguchi, J. (2007). *Mol. Genet. Genomics*, **278**, 371–383.

Hall, T. M., Porter, J. A., Beachy, P. A. & Leahy, D. J. (1995). *Nature (London)*, **378**, 212–216.

Hermoso, J. A., Garcia, J. L. & Garcia, P. (2007). *Curr. Opin. Microbiol.* **10**, 461–472.

Kabsch, W. & Sander, C. (1983). *Biopolymers*, **22**, 2577–2637.

Korndörfer, I. P., Danzer, J., Schmelcher, M., Zimmer, M., Skerra, A. & Loessner, M. J. (2006). *J. Mol. Biol.* **364**, 678–689.

La Fortelle, E. de, Irwin, J. & Bricogne, G. (1997*a*). *Crystallographic Computing 7*, edited by P. Bourne & K. Watenpaugh. Oxford: IUCr/Oxford University Press.

La Fortelle, E. de, Irwin, J. & Bricogne, G. (1997*b*). *Proceedings of the CCP4 Study Weekend. Recent Advances In Phasing*, edited by K. S. Wilson, G. Davies, A. W. Ashton & S. Bailey, pp. 25–39. Warrington: Daresbury Laboratory.

Loessner, M. J. (2005). *Curr. Opin. Microbiol.* **8**, 480–487.

Loessner, M. J., Kramer, K., Ebel, F. & Scherer, S. (2002). *Mol. Microbiol.* **44**, 335–349.

Loessner, M. J., Rees, C. E., Stewart, G. S. & Scherer, S. (1996). *Appl. Environ. Microbiol.* **62**, 1133–1140.

Loessner, M. J., Schneider, A. & Scherer, S. (1996). *Appl. Environ. Microbiol.* **62**, 3057–3060.

Loessner, M. J., Wendlinger, G. & Scherer, S. (1995). *Mol. Microbiol.* **16**, 1231–1241.

McPherson, A. (1985). *Methods Enzymol.* **114**, 112–120.

Marcyjaniak, M., Odintsov, S. G., Sabala, I. & Bochtler, M. (2004). *J. Biol. Chem.* **279**, 43982–43989.

Matthews, M. L., Periyannan, G., Hajdin, C., Sidgel, T. K., Bennett, B. & Crowder, M. W. (2006). *J. Am. Chem. Soc.* **128**, 13050–13051.

Oldfield, T. J. (2001). *Acta Cryst.* D**57**, 82–94.

Pape, T. & Schneider, T. R. (2004). *J. Appl. Cryst.* **37**, 843–844.

Perrakis, A., Morris, R. & Lamzin, V. S. (1999). *Nature Struct. Biol.* **6**, 458–463.

Ramachandran, G. N., Ramakrishnan, C. & Sasisekharan, V. (1963). *J. Mol. Biol.* **7**, 95–99.

Sambrook, J. & Russell, D. W. (2001). *Molecular Cloning: A Laboratory Manual*, 3rd ed. New York: Cold Spring Harbor Laboratory Press.

Schmidt, T. G. M. & Skerra, A. (2007). *Nature Protoc.* **2**, 1528–1535.

Skerra, A. (1994). *Gene*, **151**, 131–135.

Van Duyne, G. D., Standaert, R. F., Karplus, P. A., Schreiber, S. L. & Clardy, J. (1993). *J. Mol. Biol.* **229**, 105–124.

Zimmer, M., Sattelberger, E., Inman, R. B., Calendar, R. & Loessner, M. J. (2003). *Mol. Microbiol.* **50**, 303–317.